JOURNAL OF GUIDANCE, CONTROL, AND DYNAMICS
Vol. 18, No. 2, March–April 1995

Failure Detection and Isolation Structure for Global Positioning System Autonomous Integrity Monitoring

Ren Da* and Ching-Fang Lin†
American GNC Corporation, Chatsworth, California 91311

In this paper, a new failure detection and isolation (FDI) structure is investigated for global positioning system (GPS) integrity monitoring in an integrated inertial navigation system (INS)/GPS navigation system. In the structure, a bank of auxiliary integrated INS/GPS Kalman filters, each of them processing a subset of the GPS measurements, are applied to provide high-accuracy detection references. The failure detection is then undertaken by checking the consistency between the state estimate of the main integrated INS/GPS Kalman filter and the auxiliaries. Two state propagators are also included in the FDI structure to reliably isolate the failed GPS measurement. The two propagators are alternatively reset with the data of the Kalman filter to increase their accuracy and thereby the failure isolation performance. The failure isolation is realized by testing the consistency between the state estimates of the auxiliary Kalman filters and the state propagator. The simulation results show that the FDI structure is capable of not only detecting the presence of a malfunctioning satellite that results in a large range error, but also identifying which satellite is malfunctioning.

I. Introduction

RECENTLY, there has been considerable interest in the problem of global positioning system (GPS) integrity monitoring.[1–10] Here integrity means the system's ability to provide timely warnings to users as to when it should not be used. The main concern is over the safety in navigation with GPS and the possibility that a GPS satellite may transmit an erroneous navigation signal to the user. It is required that a GPS malfunction be detected within 10 s of the time at which the navigation accuracy is outside the defined alarm limits. Unfortunately, the GPS control segment cannot react to GPS malfunctions in this time frame. Typically, it takes the control segment from 15 min to 2 h to determine that there is a problem, identify it, determine a course of corrective action, and implement that action.[3]

Currently, there are two main methods proposed for GPS integrity monitoring. One approach uses the Wide Area Integrity Broadcast (WIB) [formerly the GPS Integrity Channel (GIC)].[1–5] The WIB uses a network of ground monitoring stations. Each of them is placed at a specific, surveyed location to determine the status of every GPS satellite in view. It will then broadcast the satellite's health to GPS users in real time from a geostationary satellite, thus providing system integrity. The other method uses receiver autonomous integrity monitoring (RAIM).[6–10] RAIM refers to a class of self-contained GPS integrity monitoring methods, which are based on a consistency check among redundant ranging signals to detect an unacceptably large satellite range error due to either satellite clock or erroneous satellite ephemeris data. Several RAIM schemes and their performance have been investigated recently, including the range and position comparison methods,[8] the least-squares residual scheme,[6] and the maximum-separation RAIM algorithm.[7] All of these RAIM approaches require at least five satellites in view. The studies to date, however, indicate that even a 21-satellite constellation with three active spares is unlikely to support RAIM a large enough fraction of the time for the application of nonprecision approaches,[3,8] which have the desired integrity performance requirements: 10 s time to alarm and 0.3-n.mi. alarm limit with misdetection probability 10^{-6}–10^{-7}.[4]

A variety of novel failure detection and isolation (FDI) approaches have been developed in recent years.[11–18] Among them, there are powerful failure detection approaches that not only avoid assumptions about how the failure components behave, but are also applicable to time-variant systems where additive process and measurement noise is present. These approaches detect failures by monitoring the consistency of the state estimates of the Kalman filter and a state propagator (or auxiliary Kalman filters) with respect to the two-ellipsoid overlap test[19] or more simply the state chi-square test (SCST).[20,21]

Based on the SCST, a structure suitable for detecting a GPS malfunction was proposed in Ref. 22. In the approach, a bank of auxiliary Kalman filters, each of them processing only subsets of system measurements, are applied to provide high-accuracy detection references. The failure detection is then undertaken by checking the consistency between the state estimate of the main Kalman filter and that of the auxiliaries.

Failure isolation is also of great importance for a GPS integrity monitoring system. After a GPS malfunction is detected, it is highly desirable to know which GPS satellite has failed and the seriousness of the failure. In this paper, a novel failure diagnosis structure is presented for GPS integrity monitoring in an integrated inertial navigation system (INS)/GPS navigation system. In this structure, not only a bank of auxiliary integrated INS/GPS Kalman filters, each of them processing only subsets of the GPS measurements, are applied to provide high-accuracy detection references, but also two state propagators are included for isolating the failed GPS measurement. Although the failure detection is undertaken by checking the consistency between the state estimate of the main integrated INS/GPS Kalman filter and the auxiliaries, the failure isolation is realized by testing the consistency between the state estimates of the auxiliary Kalman filters and the state propagators. It will be shown in the paper that the GPS integrity monitoring structure is capable of detecting the presence of a soft ramp-type GPS satellite failure well before large position estimation errors result and identifying which satellite is malfunctioning even when only four satellites are in view.

The paper is organized as follows: the integrated GPS/INS state and measurement equations are briefly described in Sec. II; the GPS autonomous integrity monitoring structure is presented in Sec. III; the numerical simulation examples are shown in Sec. IV; and an overall summary is given in Sec. V.

II. Global Positioning/Inertial Navigation System Structure

A. State Equation

The error states of a GPS/INS are usually of three kinds: 1) those describing the navigation parameter errors; 2) those describing the INS error sources, such as the gyroscope drift and acceleration errors; and 3) those describing the GPS error sources, such as the GPS

Received May 16, 1994; revision received Oct. 4, 1994; accepted for publication Oct. 18, 1994.

*Senior Researcher. Member AIAA.
†President. Associate Fellow AIAA.

receiver clock offset and clock drift. A complete picture of these errors would involve a large number of states. Due to the restriction of the on-board computation resource, reduced-order models have to be applied in practical designs. For the purpose of this analysis, a 17-state system is formulated with the error state vector being

$$\mathbf{x}(t) = [\delta r_N, \delta r_E, \delta r_D, \delta v_N, \delta v_E, \delta v_D, \phi_N, \phi_E, \phi_D, \Delta_x, \Delta_y, \Delta_z, \varepsilon_x, \varepsilon_y, \varepsilon_z, \delta b, \delta n]^T \quad (1)$$

where the subscripts N, E, and D stand for the north-east-down local level reference frame and x, y, and z for the aircraft body reference frame. The terms δr_N, δr_E, δr_D denote the INS position errors; δv_N, δv_E, δv_D the INS velocity errors; ϕ_N, ϕ_E, ϕ_D the INS attitude errors and azimuth error; Δ_x, Δ_y, Δ_z the accelerometer errors; and ε_x, ε_y, ε_z the gyroscope errors. Here, δb and δn are the GPS clock offset and clock drift. The INS navigation error model is described by the following differential equations[23]:

$$\begin{aligned}
\delta\dot{r}_N &= -\dot{\lambda}\sin L\,\delta r_E + \dot{L}\,\delta r_D + \delta v_N \\
\delta\dot{r}_E &= \dot{\lambda}\sin L\,\delta r_N + \dot{\lambda}\cos L\,\delta r_D + \delta v_E \\
\delta\dot{r}_D &= -\dot{L}\,\delta r_N + \dot{\lambda}\cos L\,\delta r_E - c_1\,\delta r_D + \delta v_D \\
\delta\dot{v}_N &= -\frac{f_D + g}{R}\delta r_N + \frac{f_E \tan L}{R}\delta r_E - (2\Omega + \dot{\lambda})\sin L\,\delta v_E \\
&\quad + \dot{L}\,\delta v_D - f_D\phi_E + f_E\phi_D + \Delta_N \\
\delta\dot{v}_E &= -\frac{f_D + g + f_N \tan L}{R}\delta r_E + (2\Omega + \dot{\lambda})\sin L\,\delta v_N \\
&\quad + (2\Omega + \dot{\lambda})\cos L\,\delta v_D + f_D\phi_N - f_N\phi_D + \Delta_E \\
\delta\dot{v}_D &= \frac{f_N}{R}\delta r_N + \frac{f_E}{R}\delta r_E + \left(\frac{2g}{R} - c_2\right)\delta r_D - \dot{L}\,\delta v_N \\
&\quad - (2\Omega + \dot{\lambda})\cos L\,\delta v_E + f_E\phi_N + f_N\phi_E + \Delta_D \\
\dot{\phi}_N &= -\frac{\Omega\sin L}{R}\delta r_N + \left(\frac{v_D}{R^2} + \frac{\dot{L}\tan L}{R}\right)\delta r_E + \frac{\dot{\lambda}\cos L}{R}\delta r_D \\
&\quad + \frac{1}{R}\delta v_E - (\Omega + \dot{\lambda})\sin L\,\phi_E + \dot{L}\,\phi_D + \varepsilon_N \\
\dot{\phi}_E &= -\frac{v_D}{R^2}\delta r_N + \frac{\dot{\lambda}\sin L}{R}\delta r_E - \frac{\dot{L}}{R}\delta r_D - \frac{1}{R}\delta v_N \\
&\quad + (\Omega + \dot{\lambda})\sin L\,\phi_N + (\Omega + \dot{\lambda})\cos L\,\phi_D + \varepsilon_E \\
\dot{\phi}_D &= -\left(\frac{\Omega\cos L}{R} + \frac{\dot{\lambda}}{R\cos L}\right)\delta r_N \\
&\quad - \frac{\tan L}{R}\left(\dot{L}\tan L + \frac{v_D}{R}\right)\delta r_E - \frac{\dot{\lambda}\sin L}{R}\delta r_D \\
&\quad - \frac{\tan L}{R}\delta v_E - \dot{L}\,\phi_N - (\Omega + \dot{\lambda})\cos L\,\phi_E + \varepsilon_D
\end{aligned} \quad (2)$$

where λ and L are the longitude and latitude angles, R the radius of Earth and Ω its angular rate, f the specific force measured by the accelerometers, and c_1 and c_2 the damping gains introduced by the altimeter damping loop of the vertical channel. The input axes of the strapped-down gyroscopes and accelerometers are assumed to be aligned with the principal axes of the aircraft. The terms, Δ_N, Δ_E, Δ_D and ε_N, ε_E, ε_D are, respectively, the errors of the accelerometers and gyroscopes mapped from the aircraft body frame into the navigation frame, using appropriate elements of the direction cosine matrix. The accelerometer and gyroscope errors in the aircraft body frame are modeled as the combination of a random bias, a white random process, and a random-walk process. Therefore we have

$$\begin{aligned}
\dot{\Delta}_i &= w_{\Delta i} \qquad (i = x, y, z) \\
\dot{\varepsilon}_i &= w_{\varepsilon i} \qquad (i = x, y, z)
\end{aligned} \quad (3)$$

where w_Δ and w_ε are white input noise processes. The GPS clock offset and drift are modeled by the equations

$$\delta\dot{b} = \delta n + w_b \qquad \delta\dot{n} = w_n \quad (4)$$

where w_b and w_n are white input noise.

B. Measurement Equation

Based on the position data indicated by the INS and the ephemeris data from the GPS receiver, the ranges from the aircraft to the four satellites being tracked can be calculated. The Kalman filter measurements y_i $(i = 1, \ldots, 4)$ for the INS/GPS are formed by the differences between the pseudoranges provided by the GPS receiver and the calculated ranges. Therefore, we have the measurement equations

$$\begin{aligned}
y_i(k) &= \cos\alpha_i(k)\delta r_N + \cos\beta_i(k)\delta r_E + \cos\gamma_i(k)\delta r_D \\
&\quad + \delta b + d_i + v_i \qquad (i = 1, \ldots, 4)
\end{aligned} \quad (5)$$

where $(\cos\alpha_i, \cos\beta_i, \cos\gamma_i)$ are the direction cosines between the line of sight from the ith satellite to the aircraft and the navigation frame, d_i the pseudorange error resulting from the satellite malfunction ($d_i = 0$ when there is no failure), and v_i the pseudorange measurement white noise.

III. Global Positioning System Integrity Monitoring Architecture

A. Failure Detection and Isolation Structure and System Observability

The proposed FDI structure for the GPS integrity monitoring system is illustrated in Fig. 1, where the measurement vectors for the Kalman filters $\mathcal{A}$, $\mathcal{B}$, $\mathcal{C}$, $\mathcal{D}$, and $\mathcal{E}$ are as follows:

$$\begin{aligned}
\mathbf{y}^{\mathcal{A}}(k) &= \begin{pmatrix} y_1 \\ y_2 \\ y_3 \\ y_4 \end{pmatrix} \qquad \mathbf{y}^{\mathcal{B}}(k) = \begin{pmatrix} y_1 \\ y_2 \\ y_3 \end{pmatrix} \qquad \mathbf{y}^{\mathcal{C}}(k) = \begin{pmatrix} y_1 \\ y_2 \\ y_4 \end{pmatrix} \\
\mathbf{y}^{\mathcal{D}}(k) &= \begin{pmatrix} y_1 \\ y_3 \\ y_4 \end{pmatrix} \qquad \mathbf{y}^{\mathcal{E}}(k) = \begin{pmatrix} y_2 \\ y_3 \\ y_4 \end{pmatrix}
\end{aligned} \quad (6)$$

The main Kalman filter $\mathcal{A}$ processes all four measurements to generate the best state estimate $\hat{x}^{\mathcal{A}}$ and its covariance $P^{\mathcal{A}}$; each of the auxiliary Kalman filters processes three out of the four GPS measurements to provide the state estimates $\hat{x}^j$ (the superscript $j = \mathcal{B}, \mathcal{C}, \mathcal{D}, \mathcal{E}$) and their covariances P^j for consistency checking. If a satellite being tracked fails, one of the auxiliary Kalman filters remains uncontaminated and, so at least one of the consistency tests is expected to signal an alarm.

As is well known, a stand-alone GPS receiver needs at least four GPS pseudorange measurements to yield three-dimensional

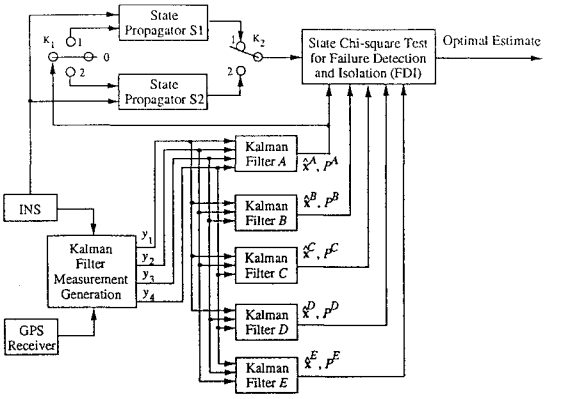

Fig. 1 An FDI structure for GPS autonomous integrity monitoring.

position navigation solution and clock bias estimate. The auxiliary filters in Fig. 1, however, use only three out of the four pseudorange measurements. It can be proven that, because of integration with the INS, these auxiliary filters can provide a complete navigation solution and a clock bias estimate. Although a complete and detailed observability proof for the auxiliary filters is beyond the scope of this paper, the following brief discussion (and our later simulation results) show that the INS position errors and GPS clock bias can be estimated with only three pseudorange measurements.

For the auxiliary filters, the parameters to be estimated do not include the position parameters, because they are already available from the INS. The main error states to be estimated are the INS position errors δr_E, δr_N, δr_D and the receiver clock bias b, which are all slowly changing parameters. For simplicity, one can treat δr_E, δr_N, δr_D, and b as constants in a short period of time ($k-m+1 \le t \le k$, k is current filtering step, and m is the sampling window width). Taking the auxiliary filter $\mathcal{B}$, for example, the measurements of the auxiliary filter $\mathcal{B}$, sampled in this period of time, can be expressed as a vector $\boldsymbol{y}_{\mathcal{B}}$:

$$\boldsymbol{y}_{\mathcal{B}} \approx H_{\mathcal{B}} \begin{pmatrix} \delta r_E \\ \delta r_N \\ \delta r_D \\ b \end{pmatrix} \tag{7}$$

where

$$\boldsymbol{y}_{\mathcal{B}} = \begin{pmatrix} y_1(k-m+1) \\ y_2(k-m+1) \\ y_3(k-m+1) \\ \vdots \\ y_1(k) \\ y_2(k) \\ y_3(k) \end{pmatrix}$$

$$H_{\mathcal{B}} = \begin{pmatrix} \cos\alpha_1(k-m+1) & \cos\beta_1(k-m+1) & \cos\gamma_1(k-m+1) & 1 \\ \cos\alpha_2(k-m+1) & \cos\beta_2(k-m+1) & \cos\gamma_2(k-m+1) & 1 \\ \cos\alpha_3(k-m+1) & \cos\beta_3(k-m+1) & \cos\gamma_3(k-m+1) & 1 \\ \vdots & \vdots & \vdots & \vdots \\ \cos\alpha_1(k) & \cos\beta_1(k) & \cos\gamma_1(k) & 1 \\ \cos\alpha_2(k) & \cos\beta_2(k) & \cos\gamma_2(k) & 1 \\ \cos\alpha_3(k) & \cos\beta_3(k) & \cos\gamma_3(k) & 1 \end{pmatrix} \tag{8}$$

Clearly, the $H_{\mathcal{B}}$ is a full-column rank matrix when $m \ge 2$, because of the relative motion between the satellites and the aircraft. Thus, the INS position errors δr_E, δr_N, δr_D and GPS clock bias b can be approximately estimated directly from Eq. (8).

The following theorem, which shows the statistical properties of the estimation differences between the Kalman filter $\mathcal{A}$ and the auxiliary Kalman filters j ($j = \mathcal{B}, \mathcal{C}, \mathcal{D}, \mathcal{E}$), provides the basis for the statistical hypothesis test.

Theorem 1. The estimation differences $\boldsymbol{b}^j$ between the Kalman filter $\mathcal{A}$ and the auxiliary Kalman filters j ($j = \mathcal{B}, \mathcal{C}, \mathcal{D}, \mathcal{E}$),

$$\boldsymbol{b}^j(k) = \hat{\boldsymbol{x}}^j(k \mid k) - \hat{\boldsymbol{x}}^{\mathcal{A}}(k \mid k) \tag{9}$$

are zero-mean Gaussian vectors with covariances

$$B^j(k) = E\{\boldsymbol{b}^j(k)[\boldsymbol{b}^j(k)]^T\} = P^j(k \mid k) - P^{\mathcal{A}}(k \mid k) \tag{10}$$

when there is no failure.

Proof. See the Appendix.

The above theorem shows that we have $\boldsymbol{b}^j \sim N[0,\ B^j(k)]$ when there is no failure. A failure will cause the expectation of $\boldsymbol{b}^j$ to become nonzero and/or its covariance larger than $B^j(k)$. Therefore, failure detection can be performed by standard statistical testing techniques between the hypotheses:

$$\begin{aligned} H_0&: \quad \boldsymbol{b}^j(k) \sim N[0,\ B^j(k)] \\ H_1&: \quad H_0 \text{ not true} \end{aligned} \tag{11}$$

subject to the false-alarm probability

$$\Pr[\text{accept } H_1 \mid H_0 \text{ true}] = \gamma \tag{12}$$

From the fact that the normalized sequence

$$\lambda^j(k) \triangleq [\boldsymbol{b}^j(k)]^T[B^j(k)]^{-1}\boldsymbol{b}^j(k) \sim \chi^2(n) \tag{13}$$

is chi-square distributed with n degrees of freedom[24] (where n is the dimension of $\boldsymbol{b}^j$), a chi-square test with the following detection rule can be utilized:

$$\zeta^j(k) \triangleq \frac{\lambda^j(k)}{\epsilon^j} \begin{cases} \ge 1 \text{ means failure} \\ < 1 \text{ means no failure} \end{cases} \tag{14}$$

where $\zeta^j(k)$ is the scaled test statistic calculated at the time k and ϵ^j the constant threshold obtained from the chi-square distribution table with the chosen false-alarm probability γ. The test is simple because $\lambda^j(k)$ can be easily calculated from $\boldsymbol{b}^j(k)$ and $B^j(k)$, which are obtained directly from the Kalman filters.

Equation (13) considers the whole vector $\boldsymbol{b}^j(k)$ as the testing object, with the advantage of including the cross correlation among the components of $\boldsymbol{b}^j(k)$. For a high-dimensional system, however, it may be better to test the components of $\boldsymbol{b}^j$ individually as

$$\lambda_l^j(k) \triangleq \frac{[b_l^j(k)]^2}{B_{ll}^j(k)} \sim \chi^2(1) \tag{15}$$

where $b_l^j(k)$ and $B_{ll}^j(k)$ are, respectively, the lth component of $\boldsymbol{b}^j(k)$ and the diagonal component of $B^j(k)$. In this way, the following two drawbacks of the previous approach can be avoided[21]: 1) the difficulty associated with the matrix inversion calculation and 2) the low detection sensitivity to failures affecting only one or few components of $\boldsymbol{b}^j(k)$. The effect of a failure on each state estimate may differ widely. Some states are affected by a failure more directly than others. The test statistic λ^j calculated by Eq. (13) reflects only the overall effects of a failure on the system state estimates, but not the individual effects on those states that are most seriously affected by the failure. Since the decision threshold ϵ^j in Eq. (14), with a chosen false-alarm probability, increases with the dimensionality of n (e.g., $\epsilon = 10.1828$ when $n = 1$ and $\epsilon = 40.490$ when $n = 17$, with the same false-alarm probability 0.001), the detection of failures that affect only a few system states may be greatly delayed or not occur.

The corresponding detection rule is

$$\zeta_l^j(k) \triangleq \frac{\lambda_l^j(k)}{\epsilon_l^j} \begin{cases} \ge 1 \text{ means failure} \\ < 1 \text{ means no failure} \end{cases} \tag{16}$$

with the constant threshold ϵ_l^j again obtained from the chi-square distribution table with the chosen false-alarm probability. With this detection rule, we can expect that the test statistic of $\zeta_l^j(k)$, which is most seriously affected by the failures, flags the failures first.

B. Failure Isolation Process

Two state propagators ($\mathcal{S}_1$, $\mathcal{S}_2$) are also included in Fig. 1 for isolating the failed GPS measurement. These two state propagators are reset alternatively with the Kalman filter data to isolate the failure.[21] Assume t_j ($j = 1, \ldots$) are the time points at which one of the state propagators is reset with the Kalman filter data and the other is put to work as the failure isolation reference. Then the switch K_1 will be at position 1 to reset the state propagator 1 when $k = t_{2i}$ ($i = 1, \ldots$), at position 2 to reset the state propagator 2 when $k = t_{2i-1}$, and at

position 0 when $k \neq t_j$ $(j = 1, \ldots)$. The switch K_2 will be at position 1 to use the state propagator 1 as the failure isolation reference when $t_{2i-1} \leq k < t_{2i}$ and at position 2 to use the state propagator 2 as the failure isolation reference when $t_{2i} \leq k < t_{2i+1}$. With this method, a newly reset state propagator does not work as the failure isolation reference right away. Only after a certain period of time $\Delta t = t_{j+1} - t_j$, when it is certain that no failure happened before the state propagator was reset, will it be put to work. In this way, the risk of using a contaminated state propagator as the failure isolation reference can be greatly minimized.

The state estimate $\hat{\boldsymbol{x}}^s(k)$ and covariance matrix $P^s(k)(s = \mathcal{S}_1, \mathcal{S}_2)$ are propagated on the sole base of the system model. Define the estimation differences between the auxiliary Kalman filters and the referenced state propagator as

$$\boldsymbol{b}^{js}(k) \triangleq \hat{\boldsymbol{x}}^j(k) - \hat{\boldsymbol{x}}^s(k \mid k) \tag{17}$$

It has been proven in Ref. 20 that

$$\boldsymbol{b}^{js}(k) \sim N[0, B^{js}(k)] \tag{18}$$

where

$$B^{js}(k) \triangleq E[\boldsymbol{b}^{js}(k)[\boldsymbol{b}^{js}(k)]^T] = P^s(k) - P^j(k \mid k) \tag{19}$$

Thus, a similar consistency testing rule as described before can be considered.

The failure isolation is then realized by testing the consistency between the state estimates of the auxiliary Kalman filters and the state propagators. No matter which GPS satellite has a failure, one of the auxiliary Kalman filters will not be contaminated, whereas the others are. Thus, when the failure happens, the consistency test between the auxiliary Kalman filter that remains uncontaminated will not signal a failure, whereas the consistency tests between the state propagators and the other contaminated auxiliary Kalman filters will signal the failure.

IV. Simulation Results and Discussions

In simulation, the components of $\boldsymbol{b}^j$ (or $\boldsymbol{b}^{js}$) were tested separately and the scaled test statistics were used. All the thresholds ϵ_i^j in Eq. (16) were chosen as $\epsilon = 7.87944$, corresponding to a false-alarm probability of 0.005. Table 1 lists the initial variances and parameters of the error states to be used in the simulation analysis. The mission scenario was 800 s of flight toward west at a constant flight speed of 300 m/s.

The effectiveness of the GPS integrity monitoring system was investigated by assuming that the failure in satellite 4 resulted in the following ramp-type pseudorange errors:

$$d_4 = \begin{cases} 0 \text{ m} & 0 \text{ s} \leq t < 500 \text{ s} \\ 5(t - 500) \text{ m} & 500 \text{ s} \leq t < 510 \text{ s} \\ 50 \text{ m} & 510 \text{ s} \leq t \leq 800 \text{ s} \end{cases} \tag{20}$$

Table 1 Modeling parameter list

Error source	Value (1σ)	Units
Initial position errors $\delta r_N, \delta r_W, \delta r_Z$	100.0	m
Initial velocity errors $\delta v_N, \delta v_W, \delta v_Z$	1.0	m/s
Initial attitude errors ϕ_N, ϕ_W	300.0	arcsec
Initial azimuth error ϕ_Z	900.0	arcsec
Accelerometer errors $\Delta_x, \Delta_y, \Delta_z$	500.0	μg
Accelerometer white noise	5.0	$\mu g \cdot s^{1/2}$
Gyroscope errors $\varepsilon_x, \varepsilon_y, \varepsilon_z$	0.1	deg/h
Gyroscope white noise	0.001	deg/h$^{1/2}$
GPS clock offset bias	30	m
GPS clock offset noise w_b	0.1	m $\cdot$ s$^{1/2}$
GPS clock drift δn	0.1	m/s
GPS pseudorange noise	10	m

A. Failure Detection Results

Our discussion of failure detection will concentrate on the consistency test results associated with the main Kalman filter $\mathcal{A}$ and the auxiliary filter $\mathcal{B}$, which is the only one uncontaminated when satellite 4 fails, and on the results related to the position errors, which are not only the most important parameters for practical navigation systems, but also those most seriously affected by the GPS pseudorange failures. The results related to most of the other error states will be omitted for better clarity.

Figure 2 shows the real north-position estimation errors $\tilde{\delta} r_N^{\mathcal{A}}$ as well as the standard derivation $\sqrt{P_{\delta r_N}^{\mathcal{A}}}$ from the Kalman filter $\mathcal{A}$. Under normal working status ($t \leq 500$ s) the $\tilde{\delta} r_N^{\mathcal{A}}$ (solid line) is mainly limited within the scope $\pm\sqrt{P_{\delta r_N}^{\mathcal{A}}}$ (dashed line). Once the failure happens at $t = 500$ s, the $\tilde{\delta} r_N^{\mathcal{A}}$ increases rapidly and soon exceeds that scope.

The real state estimation errors are not known in the practical Kalman filter systems because the real system states are not known. Hence, some kind of reference systems are always needed in order to monitor the real estimation errors indirectly. Figure 3 indicates that the Kalman filter $\mathcal{B}$, not contaminated by the failed measurement y_4, provides an excellent reference system. Using three out of the four pseudorange measurements, the accuracy of the Kalman filter $\mathcal{B}$ is fairly high. The difference between the covariance $P_{\delta r_N}^{\mathcal{B}}$ and $P_{\delta r_N}^{\mathcal{A}}$, for example, is less than 5 m^2 before the failure happens. Therefore, the plot of $b_{\delta r_N}^{\mathcal{B}}$ (see Fig. 4),

$$b_{\delta r_N}^{\mathcal{B}} = \hat{\delta} r_N^{\mathcal{B}} - \hat{\delta} r_N^{\mathcal{A}} = \tilde{\delta} r_N^{\mathcal{A}} - \tilde{\delta} r_N^{\mathcal{B}} \tag{21}$$

behaves like $\tilde{\delta} r_N^{\mathcal{A}}$ (Fig. 2) after the failure happens, because

$$\tilde{\delta} r_N^{\mathcal{A}} \gg \tilde{\delta} r_N^{\mathcal{B}} \qquad b_{\delta r_N}^{\mathcal{B}} \approx \tilde{\delta} r_N^{\mathcal{A}} \tag{22}$$

In practical applications, it is often desirable to know approximately the magnitudes of the real state estimation errors in order to decide the seriousness of the failures detected. This can be done on the basis

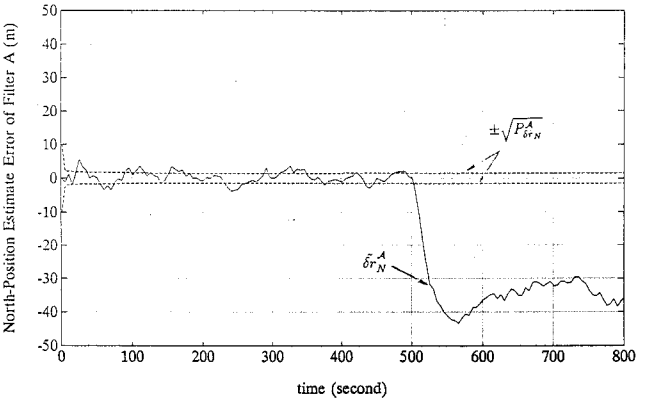

Fig. 2 North-position estimation errors $\tilde{\delta} r_N^{\mathcal{A}}$ (solid line) and $\pm\sqrt{P_{\delta r_N}^{\mathcal{A}}}$ (dashdot lines) of the Kalman filter $\mathcal{A}$.

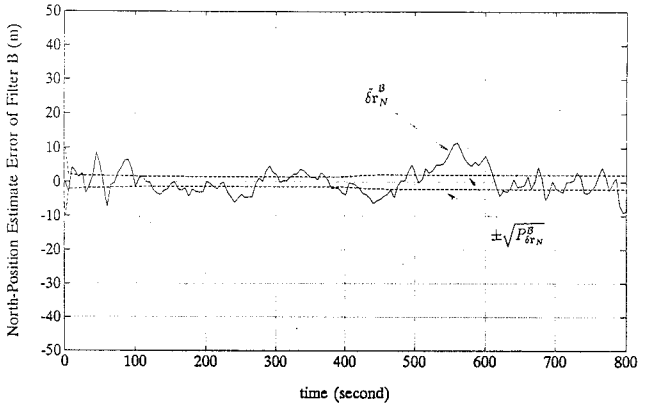

Fig. 3 North-position estimation error $\tilde{\delta} r_N^{\mathcal{B}}$ (solid line) and $\pm\sqrt{P_{\delta r_N}^{\mathcal{B}}}$ (dashdot lines) of the Kalman filter $\mathcal{B}$.

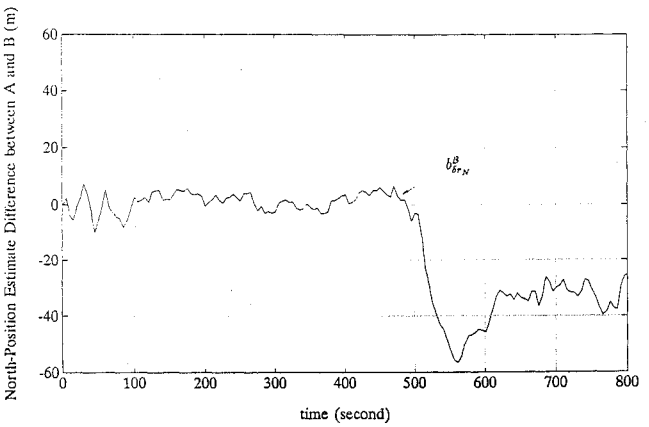

Fig. 4 North-position estimation difference $\hat{\delta r}_N^{\mathcal{B}} - \hat{\delta r}_N^{\mathcal{A}}$ between Kalman filter $\mathcal{A}$ and Kalman filter $\mathcal{B}$.

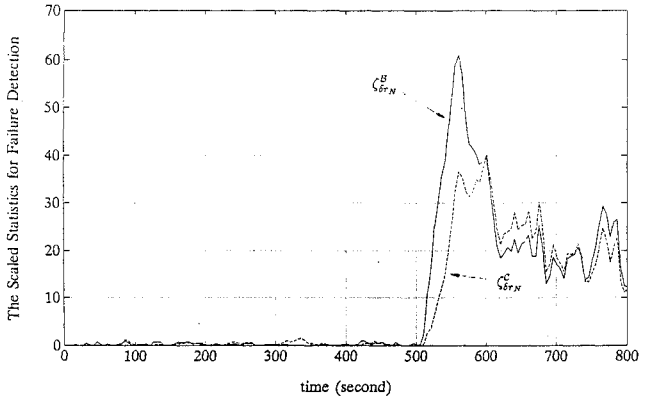

Fig. 5 Consistency testing results $\zeta_{\delta r_N}^{\mathcal{B}}$ (solid line) between Kalman filter $\mathcal{A}$ and Kalman filter $\mathcal{B}$ as well as result $\zeta_{\delta r_N}^{\mathcal{C}}$ (dashed line) between Kalman filter $\mathcal{A}$ and Kalman filter $\mathcal{C}$.

of the information provided by the Kalman filters. For example, the magnitudes of the real north-position estimation error can be estimated by the inequality (with probability 0.9973)

$$\begin{aligned} \left|\tilde{\delta r}_N^{\mathcal{A}}\right| &= \left|\delta r_N - \hat{\delta r}_N^{\mathcal{A}}\right| \\ &\le \left|\delta r_N - \hat{\delta r}_N^{\mathcal{B}}\right| + \left|\hat{\delta r}_N^{\mathcal{B}} - \hat{\delta r}_N^{\mathcal{A}}\right| \\ &< 3\sqrt{P_{\delta r_N}^{\mathcal{B}}} + \left|\hat{\delta r}_N^{\mathcal{B}} - \hat{\delta r}_N^{\mathcal{A}}\right| \end{aligned} \tag{23}$$

Thus the maximum $|\tilde{\delta r}_N^{\mathcal{A}}|$ is calculated to be less than 60 m (with probability 0.9973), based on the data of $\hat{\delta r}_N^{\mathcal{A}}$, $P_{\delta r_N}^{\mathcal{B}}$, and $\hat{\delta r}_N^{\mathcal{B}}$ from the filters $\mathcal{A}$ and $\mathcal{B}$.

Figure 5 plots the consistency testing results of the north-position error for the failure case. As expected, the scaled chi-square test statistics $\zeta_{\delta r_N}^{\mathcal{B}}$,

$$\zeta_{\delta r_N}^{\mathcal{B}} = \frac{\left(\hat{\delta r}_N^{\mathcal{A}} - \hat{\delta r}_N^{\mathcal{B}}\right)^2}{\epsilon\left(P_{\delta r_N}^{\mathcal{B}} - P_{\delta r_N}^{\mathcal{A}}\right)} \tag{24}$$

increases rapidly with accumulation of the failure effects on the north-position estimation (solid line). When the SCST statistics $\zeta_{\delta r_N}^{\mathcal{B}}$ are larger than 1, the failures are declared. When the failure is declared, the real estimation error $\tilde{\delta r}_N^{\mathcal{A}}$ is less than 15 m. Hence, the failure detection system is quite sensitive to the GPS pseudorange failures, which can be detected well before large position estimation errors result.

The simulation results also show that not only the consistency tests between the Kalman filters $\mathcal{A}$ and $\mathcal{B}$, but also those between the Kalman filter $\mathcal{A}$ and others may signal failures. For example, although the filters $\mathcal{A}$ and $\mathcal{C}$ are affected by the same satellite failure, the estimation difference between $\hat{\delta r}_N^{\mathcal{A}}$ and $\hat{\delta r}_N^{\mathcal{C}}$ is still large enough to cause the scaled test statistics $\zeta_{\delta r_N}^{\mathcal{C}}$ to signal the failure, as shown

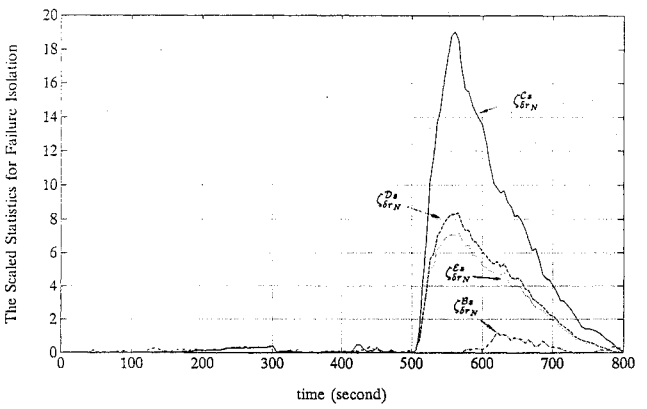

Fig. 6 Consistency testing results between auxiliary filters and state propagators.

in Fig. 5 (dashed line). Thus, it is difficult for us to tell which GPS satellite has a failure based only on the consistency tests between the Kalman filters.

B. Failure Isolation Results

The consistency tests between the auxiliary Kalman filters and the state propagators provide us the possibility to further isolate the failed GPS satellites. Figure 6 shows the consistency testing results associated with the auxiliary filters and the state propagators, where

$$\zeta_{\delta r_N}^{js} = \frac{\left(\hat{\delta r}_N^{j} - \hat{\delta r}_N^{s}\right)^2}{\epsilon\left(P_{\delta r_N}^{s} - P_{\delta r_N}^{j}\right)} \qquad (j = \mathcal{B}, \mathcal{C}, \mathcal{D}, \mathcal{E}) \tag{25}$$

The simulation results show that statistic $\zeta^{\mathcal{B}s}$ between the auxiliary filter $\mathcal{B}$ and the state propagators is evidently much smaller than the test statistic $\zeta_{\delta r_N}^{ps}$ $(p = \mathcal{C}, \mathcal{D}, \mathcal{E})$ between other auxiliary filters and the state propagators. The consistency testing results between the state propagators and the auxiliary filters $\mathcal{C}$, $\mathcal{D}$, $\mathcal{E}$, except the consistency testing result between the state propagators and the auxiliary filter $\mathcal{B}$, which is the only one uncontaminated when satellite 4 fails, show something is wrong in the system. Therefore, the failed satellite 4 is isolated.

C. Discussion

Several important issues are worthwhile to be discussed:

1) The GPS integrity monitoring system is quite sensitive to the GPS pseudorange failures, which can be detected well before large position estimation errors result. The simulation results show that the real estimation error $\tilde{\delta r}_N^{\mathcal{A}}$ is less than 15 m when the failure is detected. This is much smaller than the integrity monitoring requirement of 0.3-n.mi. alarm limit for a nonprecision approach.

2) The system needs only the measurements from four satellites in view, whereas most currently published RAIM approaches require the measurements from at least five satellites.

3) In this investigation, we use only the pseudorange measurements. One may also include delta range measurements in order to increase the system performance.

4) The investigations in this paper assume accurate knowledge of the system dynamics. Modeling errors, however, may degrade the performance of the chi-square test.[25] A sensitivity analysis algorithm, which provides a tool for statistical analysis of the impact of modeling errors on the SCST approach presented in the paper, is now available in Ref. 26.

5) Although the simulation results have shown that the proposed approach is very sensitive to satellite failures and can detect them far before large position errors result, more investigations are necessary to test its possibility of misdetection and misisolation.

V. Conclusion

A new FDI structure is presented for GPS integrity monitoring in an integrated INS/GPS navigation system. It exploits the concepts of using a bank of auxiliary integrated INS/GPS Kalman filters, each of them processing a subset of the GPS measurements, to provide

high-accuracy detection references and detecting GPS failures by checking the consistency between the state estimate of the main integrated GPS/INS Kalman filter and those of the auxiliaries. Two state propagators are also included in the FDI structure to reliably isolate the failed GPS measurement. The failure isolation is realized by testing the consistency between the state estimates of the auxiliary Kalman filters and the state propagator. The simulation results demonstrate that the FDI structure is capable of not only detecting the presence of a soft ramp-type GPS satellite failure well before large position estimation errors result, but also of identifying which satellite is malfunctioning.

Appendix: Proof of Theorem 1

Let

$$\tilde{\boldsymbol{x}}^i(k \mid k) \triangleq \boldsymbol{x}(k) - \hat{\boldsymbol{x}}^i(k \mid k) \tag{A1}$$

$$P^i(k \mid k) \triangleq E\{\tilde{\boldsymbol{x}}^i(k \mid k)[\tilde{\boldsymbol{x}}^i(k \mid k)]^T\} \tag{A2}$$

where $i = \mathcal{A}, \mathcal{B}, \mathcal{C}, \mathcal{D}, \mathcal{E}$, and

$$\begin{aligned} \boldsymbol{b}^j(k) &\triangleq \hat{\boldsymbol{x}}^j(k \mid k) - \hat{\boldsymbol{x}}^{\mathcal{A}}(k \mid k) \\ &= [\boldsymbol{x}(k) - \hat{\boldsymbol{x}}^{\mathcal{A}}(k \mid k)] - [\boldsymbol{x}(k) - \hat{\boldsymbol{x}}^j(k \mid k)] \\ &= \tilde{\boldsymbol{x}}^{\mathcal{A}}(k \mid k) - \tilde{\boldsymbol{x}}^j(k \mid k) \end{aligned} \tag{A3}$$

where $j = \mathcal{B}, \mathcal{C}, \mathcal{D}, \mathcal{E}$. When there is no failure, all the state estimates from the Kalman filters are unbiased, so

$$E[\boldsymbol{b}^j(k)] = E[\tilde{\boldsymbol{x}}^{\mathcal{A}}(k \mid k)] - E[\tilde{\boldsymbol{x}}^j(k \mid k)] = 0 \tag{A4}$$

The covariance for $\boldsymbol{b}^j(k)$ can be derived with an application of the orthogonal projection principle. In fact, introducing a normed state space X, $\boldsymbol{x}(k) \in X$, and the subspaces $Y^i(k)$ $(i = \mathcal{A}, \mathcal{B}, \mathcal{C}, \mathcal{D}, \mathcal{E})$, where

$$Y^i(k) = \{\text{subspace spanned by } \boldsymbol{x}_0,\ \boldsymbol{y}^i(1), \ldots, \boldsymbol{y}^i(k)\} \tag{A5}$$

it follows from the orthogonal projection principle[27] that the optimal state estimate $\hat{\boldsymbol{x}}^i(k \mid k)$ is the orthogonal projection of $\boldsymbol{x}(k)$ into the subspace $Y^i(k)$, or the estimation error $\tilde{\boldsymbol{x}}^i(k \mid k)$ is orthogonal to $Y^i(k)$:

$$E[\tilde{\boldsymbol{x}}^i(k \mid k)\alpha^T(k)] = 0 \qquad \text{for all} \qquad \alpha(k) \in Y^i(k) \tag{A6}$$

From Eq. (A3), the covariance $B^j(k)$ of $\boldsymbol{b}^j(k)$ is written as

$$\begin{aligned} B^j(k) &\triangleq E\{\boldsymbol{b}^j(k)[\boldsymbol{b}^j(k)]^T\} \\ &= P^{\mathcal{A}}(k \mid k) + P^j(k \mid k) - E\{\tilde{\boldsymbol{x}}^{\mathcal{A}}(k \mid k)[\tilde{\boldsymbol{x}}^j(k \mid k)]^T\} \\ &\quad - E\{\tilde{\boldsymbol{x}}^j(k \mid k)[\tilde{\boldsymbol{x}}^{\mathcal{A}}(k \mid k)]^T\} \end{aligned} \tag{A7}$$

where

$$\begin{aligned} &E\{\tilde{\boldsymbol{x}}^j(k \mid k)[\tilde{\boldsymbol{x}}^{\mathcal{A}}(k \mid k)]^T\} \\ &= E\{\{[\boldsymbol{x}(k) - \hat{\boldsymbol{x}}^{\mathcal{A}}(k \mid k)] \\ &\quad + E\hat{\boldsymbol{x}}^{\mathcal{A}}(k \mid k) - \hat{\boldsymbol{x}}^j(k \mid k)]\}[\tilde{\boldsymbol{x}}^{\mathcal{A}}(k \mid k)]^T\} \\ &= P^{\mathcal{A}}(k \mid k) + E\{[\hat{\boldsymbol{x}}^{\mathcal{A}}(k \mid k) - \hat{\boldsymbol{x}}^j(k \mid k)][\tilde{\boldsymbol{x}}^{\mathcal{A}}(k \mid k)]^T\} \end{aligned} \tag{A8}$$

Since

$$\hat{\boldsymbol{x}}^j(k \mid k) \in Y^j(k) \subset Y^{\mathcal{A}}(k) \tag{A9}$$

$$\hat{\boldsymbol{x}}^{\mathcal{A}}(k \mid k) - \hat{\boldsymbol{x}}^j(k \mid k) \in Y^{\mathcal{A}}(k) \tag{A10}$$

we have, from Eq. (A6),

$$E\{[\hat{\boldsymbol{x}}^{\mathcal{A}}(k \mid k) - \hat{\boldsymbol{x}}^j(k \mid k)][\tilde{\boldsymbol{x}}^{\mathcal{A}}(k \mid k)]^T\} = 0 \tag{A11}$$

With Eqs. (A11) and (A8),

$$\begin{aligned} &E\{[\tilde{\boldsymbol{x}}^j(k \mid k)][\tilde{\boldsymbol{x}}^{\mathcal{A}}(k \mid k)]^T\} \\ &= E\{[\tilde{\boldsymbol{x}}^{\mathcal{A}}(k \mid k)][\tilde{\boldsymbol{x}}^j(k \mid k)]^T\} = P^{\mathcal{A}}(k \mid k) \end{aligned} \tag{A12}$$

Substituting Eq. (A12) into Eq. (A7), we finally have the following simple equation for the covariance $B^j(k)$:

$$B^j(k) = E\{[\boldsymbol{b}^j(k)][\boldsymbol{b}^j(k)]^T\} = P^j(k \mid k) - P^{\mathcal{A}}(k \mid k) \tag{A13}$$

Therefore, the estimation differences $\boldsymbol{b}^j(k)$ are Gaussian vectors with zero-mean and variances $B^j(k)$ under normal working status.

Acknowledgments

The authors thank I. Y. Bar-Itzhack of the Technion for his comments and suggestions. The clarity of this paper has been substantially improved after comments on a first submission by the associate editor D. G. Denery and two anonymous reviewers, which the authors gratefully acknowledge.

References

[1]Braff, R., and Shively, C., "GPS Integrity Channel," *Navigation: Journal of the Institute of Navigation*, Vol. 32, No. 4, 1985, pp. 334–350.

[2]Jorgensen, P. S., "Achieving GPS Integrity and Eliminating Areas of Degraded Performance," *Navigation: Journal of the Institute of Navigation*, Vol. 34, No. 4, 1987, pp. 297–306.

[3]Kalafus, R. H., "GPS Integrity Channel RTCA Working Group Recommendations," *Navigation: Journal of the Institute of Navigation*, Vol. 36, No. 1, 1989, pp. 25–44.

[4]Loh, R., and Fernow, J. P., "Integrity Monitoring Requirements for FAA's GPS Wide-Area Augmentation System (WAAS)," *Proceedings of IEEE Position, Location, and Navigation Symposium*, April 1994, pp. 629–636.

[5]Van Dierendonck, A. J., and Enge, P., "RTCA SC-159 Wide Area Integrity Broadcast/Wide Area Differential GPS Status," *Proceedings of IEEE Position, Location, and Navigation Symposium*, April 1994, pp. 733–738.

[6]Parkinson, B., and Axelrad, P.,"Autonomous GPS Integrity Monitoring Using the Pseudorange Residual," *Navigation: Journal of the Institute of Navigation*, Vol. 35, No. 2, 1988, pp. 255–274.

[7]Brown, R. G., "A Baseline GPS RAIM Scheme and a Note on the Equivalence of Three RAIM Methods," *Navigation: Journal of the Institute of Navigation*, Vol. 39, No. 3, 1992, pp. 301–316.

[8]Lee, Y. C., "Receiver Autonomous Integrity Monitoring (RAIM) Capability for Sole-Means GPS Navigation in the Oceanic Phase of Flight," *Proceedings of the IEEE Position, Location, and Navigation Symposium*, 1992, pp. 464–465.

[9]Von Diggelen, F., and Brown, A., "Mathematical Aspects of GPS RAIM," *Proceedings of IEEE Position, Location, and Navigation Symposium*, April 1994, pp. 733–738.

[10]Pullen, S. P., Pervan, B. S., and Parkinson, B. W., "A New Approach to GPS Integrity Monitoring Using Prior Probability Models and Optimal Threshold Search," *Proceedings of IEEE Position, Location, and Navigation Symposium*, April 1994, pp. 739–746.

[11]Willsky, A. S., "A Survey of Design Methods for Failure Detection in Dynamic Systems," *Automatica*, Vol. 12, 1976, pp. 601–611.

[12]Isermann, R., "Process Fault Detection Based on Modeling and Estimation Methods: A Survey," *Automatica*, Vol. 20, No. 4, 1984, pp. 387–404.

[13]Kerr, T. H., "Decentralized Kalman Filtering and Redundancy Management for Multisensor Navigation," *IEEE Transactions on Aerospace and Electronic Systems*, Vol. 23, No. 1, 1987, pp. 83–119.

[14]Gertler, J. J., "Survey of Model Based Failure Detection and Isolation in Complex Plants," *IEEE Control Systems Magazine*, Vol. 8, No. 6, 1988, pp. 3–11.

[15]Frank, P. M., "Fault Diagnosis in Dynamic System Using Analytical and Knowledge-Based Redundancy: A Survey and Some New Results," *Automatica*, Vol. 26, No. 1, 1990, pp. 459–474.

[16]Patton, R. J., and Chen, J., "Review of Parity Approaches to Fault Diagnosis for Aerospace Systems," *Journal of Guidance, Control, and Dynamics*, Vol. 17, No. 2, 1994, pp. 278–285.

[17]Lin, C. F., *Modern Navigation, Guidance, and Control Processing*, Prentice–Hall Series in Advanced Navigation, Guidance, and Control, and their Applications, Prentice–Hall, Englewood Cliffs, NJ, 1991.

[18]Lin, C. F. (ed.), *Advanced Control System Design*, Prentice–Hall Series in Advanced Navigation, Guidance, and Control, and their Applications, Prentice–Hall, Englewood Cliffs, NJ, 1994.

[19]Kerr, T. H., "Statistical Analysis of a Two-Ellipsoid Overlap Test for Real-Time Failure Detection," *IEEE Transactions on Automatic Control*, Vol. 25, No. 4, 1980, pp. 762–772.

[20]Brumback, B. D., and Srinath, M. D., "Fault-Tolerant Multisensor Nav-

igation System Design," *IEEE Transactions on Aerospace and Electronic Systems*, Vol. 23, No. 6, 1987, pp. 738–755.

[21]Da, R., "Failure Detection of Dynamical Systems with State Chi-Square Test," *Journal of Guidance, Control, and Dynamics*, Vol. 17, No. 2, 1994, pp. 271–277.

[22]Da, R., and Lin, C. F., "A New Failure Detection Approach and Its Application to GPS Autonomous Integrity Monitoring," *IEEE Transactions on Aerospace System and Electronic Systems*, Vol. 31, No. 1, 1995, pp. 499–506.

[23]Bar-Itzhack, I. Y., "Minimal Order Time Sharing Filters for INS In-Flight Alignment," *Journal of Guidance, Control, and Dynamics*, Vol. 5, No. 4, 1982, pp. 396–402.

[24]Mendenhall, W., and Sincich, T., *Statistics for Engineering and the Science*, 5th ed., Dellen, San Francisco, 1992.

[25]Mangoubi, R., Appleby, B., and Farrell, J., "Robust Estimation in Fault Detection," *Proceedings of the Thirty-First Conference on Decision and Control*, 1992, pp. 2317–2322.

[26]Da, R., and Lin, C. F., "A Sensitivity Analysis Algorithm for the State Chi-Square Test," *Journal of Guidance, Control, and Dynamics* (submitted for publication).

[27]Jazwinski, A. H., *Stochastic Processes and Filtering Theory*, Academic, New York, 1970.